Pergamon

Int. J. Heat Mass Transfer. Vol. 40, No. 7, pp. 1667–1675, 1997

0017–9310/97 $17.00+0.00

PII: S0017-9310(96)00216-5

Suppression of temperature oscillation in Czochralski convection by superimposing rotating flows

JUNG-IL CHOI and HYUNG JIN SUNG†

Department of Mechanical Engineering, Korea Advanced Institute of Science and Technology, 373-1, Kusong-dong, Yusong-ku, Taejon 305-701, Korea

(*Received* 18 *January* 1996)

Abstract—A numerical study was made of a control technique of transient oscillatory flows in Czochralski convection. The suppression of temperature oscillation was achieved by changing the rotation rate of crystal rod $\Omega = \Omega_0(1 + A_S \sin(2\pi/t_p f_S t))$, where A_S denotes the dimensionless rotation amplitude and f_S the frequency. Based on the inherent oscillatory time period of the melt (t_p), the suppression rate of temperature oscillation was characterized by the mixed convection parameter $Ra/(Pr\ Re^2)$. This parameter ranged in the study $0.225 \leqslant Ra/(Pr\ Re^2) \leqslant 0.929$, which encompasses the buoyancy- and forced-convection dominant regimes. Computational results revealed that the temperature oscillation can be suppressed significantly by adjusting the control parameters. The uniformity of temperature distribution in space and in time near the crystal interface was scrutinized. Copyright © 1996 Elsevier Science Ltd.

1. INTRODUCTION

Recent advances in microelectronic technologies have expanded the interests in growing high-purity single crystals. The majority of single crystals are produced in industry by the Czochralski process. In this method, the silicon crystal is contained in a heated crucible. The crystal is suspended from above and is pulled upward as it grows. The entire system rotates steadily about the vertical central axis [1]. The rotation is intended to provide additional means of control of the whole dynamic system.

It is known that high quality of the crystal can be achieved by a fluid flow field in the melt. In the Czochralski process, convection is generally driven by buoyancy and rotations of the crystal and crucible. These mutual interactions cause extreme complexities in the problem. Inhomogeneity stemming from varying impurity concentrations, which is customarily known as the growth striation, is generated in the crystal when the growth conditions are not time-invariant. These striations affect significantly the quality of the crystal, and microdefects in Czochralski silicon crystals are detrimental to the electronic properties of the device [2]. The striation is undesirable in semiconductors because it results in fluctuations of resistivity along the length of the crystal [3]. The present study aims to suppress the phenomena of temperature oscillation in convection.

A literature survey reveals that there have been considerable efforts to minimize striations, i.e. bands of high impurity or dopant concentration. Some modifications of the basic Czochralski technique have been introduced to improve the crystal quality. An overview was given in Langlois [4]. Among the techniques in the literature, one of the most significant developments is the introduction of the melt convection control by imposing magnetic fields [3–7]. The basic concept is to reduce convection in the melt, where an improvement in the micro-homogeneity of dopant distribution can be accomplished by altering the orientation and the strength of magnetic field. However, this technique has not been practically used in industry for various reasons. Another approach to alleviating the melt fluctuations is the crystal growing in a microgravity environment [5]. However, this method is also expensive due to difficulties in reducing the gravity.

As stated in the above, existing techniques to resolve the striation problems have concentrated on the reduction of convection. As an alternative promising approach to homogenization of Czochralski growth, the introduction of forced convection by periodically varying the crystal rotation rate is employed in the present study [8]. This is termed 'the accelerated crystal rotation technique', which is referred to as ACRT hereafter. The basic rationale is that an optimal stirring in the crucible can be achieved by changing the rotation rate of the crystal. It should be noted that, since the rotation rates are easily manipulated by a simple electronic device and mechanical means, it is capable of saving the cost of operation and equipment compared to the previous techniques. Some prior researches have been carried out on this method experimentally and numerically [8–13]. However, most of these studies were attempted without a sufficient

† Author to whom correspondence should be addressed.

NOMENCLATURE

A_S	amplification factor of crystal rod
f_S	frequency factor of crystal rod
g	gravitational acceleration
H	melt height
Ma	Marangoni number, $-\partial\sigma/\partial T(\Delta TH/\mu\alpha)$
R_C	crucible radius
R_S	crystal radius
Ra	Rayleigh number, $\beta g\Delta TH^3/\alpha\nu$
Re	rotational Reynolds number of crystal rod, $\Omega_{S0}H^2/\nu$
r	dimensionless radial space coordinate
T	temperature
t	dimensionless time
u	dimensionless radial velocity component
v	dimensionless azimuthal velocity component
w	dimensionless axial velocity component
z	dimensionless axial space coordinate.

Greek symbols

α	thermal diffusivity
β	volumetric thermal expansion coefficient
Γ	swirl velocity, rv
ν	kinematic viscosity
θ	dimensionless temperature
ρ	density
σ	surface tension
Ω_S	rotation rate of crystal rod with ACRT
Ω_{S0}	rotation rate of crystal rod without ACRT
ω	vorticity, $\omega/r = \partial w/\partial r - \partial u/\partial z$
ψ	meridional stream function.

Superscript

*	dimensional variable.

knowledge of the fluid flow phenomena, i.e. the inherent time period of melt oscillations was not fully taken into consideration. Recently, Sung *et al.* [14] made a systematical study on the oscillatory transient flow in a Czochralski model. The temperature oscillations were computed over a broad range of the mixed convection parameter $0.225 \leqslant Ra/PrRe^2 \leqslant 0.929$. They clarified that the oscillatory flows are essential characteristics in Czochralski convection system, and these bring forth the major cause of striations. The computed periods of oscillation were shown to be in excellent agreement with the experimental results of Ozoe *et al.* [15].

Based on the preceding numerical attempt by Sung *et al.* [14], the aforesaid ACRT is imposed in the present study. The main attention is directed to the suppression of temperature oscillation by changing the rotation rates, $\Omega_S = \Omega_{S0}(1 + A_S\sin(2\pi/t_p f_S t))$, where Ω_{S0} represents the constant rotation rate of crystal rod without the application of ACRT. The inherent oscillatory time period of the melt, which is denoted by t_p, is the key parameter to apply the ACRT in the present treatise. An assessment is made of the optimal values to suppress the temperature oscillations, i.e. the amplification factor (A_S) and frequency factor (f_S) of ACRT. For the flow geometry of present concern, the axisymmetric flow in cylindrical geometry is dealt with.

2. NUMERICAL SIMULATION

Consider a viscous incompressible fluid of kinematic viscosity ν contained in a cylindrical crucible of height H and radius R_C. The radius of the crystal rod is R_S. The flow and temperature fields are assumed to be axisymmetric with respect to the vertical central axis (z). Since the rotation speed of crystal (Ω_S) is relatively low, the free-surface of the melt is taken to be plane and adiabatic [14]. A schematic diagram of the model is shown in Fig. 1.

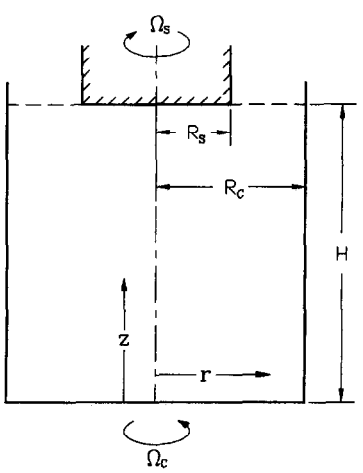

Fig. 1. Schematic diagram of the model.

The governing equations, in dimensionless form, are as follows:

$$\frac{\partial\omega}{\partial t} + \frac{\partial(u\omega)}{\partial r} + \frac{\partial(w\omega)}{\partial z} = \frac{1}{Re}\left[r\frac{\partial}{\partial r}\left(\frac{1}{r}\frac{\partial\omega}{\partial r}\right) + \frac{\partial^2\omega}{\partial z^2}\right] + \frac{Ra}{PrRe^2}r\frac{\partial\theta}{\partial r} - \frac{2\Gamma}{r^2}\frac{\partial\Gamma}{\partial z} + \frac{\omega u}{r} \quad (1)$$

$$\frac{\partial \Gamma}{\partial t}+\frac{\partial(u\Gamma)}{\partial r}+\frac{\partial(w\Gamma)}{\partial z}=\frac{1}{Re}\left[r\frac{\partial}{\partial r}\left(\frac{1}{r}\frac{\partial \Gamma}{\partial r}\right)+\frac{\partial^2\Gamma}{\partial z^2}\right]-\frac{u\Gamma}{r} \tag{2}$$

$$\frac{\partial \theta}{\partial t}+\frac{1}{r}\frac{\partial(ru\theta)}{\partial r}+\frac{\partial(w\theta)}{\partial z}=\frac{1}{Pr\,Re}\left[\frac{1}{r}\frac{\partial}{\partial r}\left(r\frac{\partial \theta}{\partial r}\right)+\frac{\partial^2\theta}{\partial z^2}\right] \tag{3}$$

$$\frac{\partial}{\partial r}\left(\frac{1}{r}\frac{\partial \psi}{\partial r}\right)+\frac{\partial}{\partial z}\left(\frac{1}{r}\frac{\partial \psi}{\partial z}\right)=\frac{\omega}{r}. \tag{4}$$

For a rotationally symmetric flow, computation time can be reduced if the problem is formulated by using the vorticity (ω) and stream function (ψ), which are defined as

$$\frac{\omega}{r}=\frac{\partial w}{\partial r}-\frac{\partial u}{\partial z},\quad u=-\frac{1}{r}\frac{\partial \psi}{\partial z},\quad w=\frac{1}{r}\frac{\partial \psi}{\partial r}. \tag{5}$$

Here, the velocity components (u, v, w) in the cylindrical coordinate system represent the radial, azimuthal and axial velocities, respectively. The swirl velocity Γ in equation (2) is $\Gamma = rv$. The equations have been made dimensionless by adopting the following non-dimensional quantities: $(r, z) = (r^*, z^*)/H$, $t = t^*(\Omega_{S0})$, $(u, v, w) = (u^*, v^*, w^*)/\Omega_{S0}H$, $\theta = (T - T_C)/(T_H - T_C)$, in which the asterisk denotes the dimensional counterparts. The following three non-dimensional parameters emerge in the governing equations, *Re*, *Pr* and *Ra*. *Re* represents the rotational Reynolds number of the crystal $Re = \Omega_{S0}H^2/\nu$, *Pr* is the Prandtl number $Pr = \nu/\alpha$ and *Ra* is the Rayleigh number $Ra = \beta g(T_H - T_C)H^3/\alpha\nu$.

In accordance with the afore-stated ACRT rationale, the boundary and the growth interface conditions are written as

$z = 0, 0 < r < R_C/H$:

$$\psi = 0,\quad \frac{\partial \psi}{\partial r}=\frac{\partial \psi}{\partial z}=0,\quad \Gamma = 0,\quad \theta = 1 \tag{6}$$

$z = 1, 0 < r < R_S/H$:

$$\psi = 0,\quad \frac{\partial \psi}{\partial r}=\frac{\partial \psi}{\partial z}=0, \tag{7}$$

$$\Gamma=\left[1+A_S\sin\left(\frac{2\pi}{t_p}f_S t\right)\right]r^2,\quad \theta = 0$$

$z = 1, R_S/H < r < R_C/H$:

$$\psi = 0,\quad \omega=\frac{Ma}{Pr\,Re}r\frac{\partial \theta}{\partial r},\quad \frac{\partial \Gamma}{\partial z}=0,\quad \frac{\partial \theta}{\partial z}=0 \tag{8}$$

$r = 0, 0 < z < 1$:

$$\psi = 0,\quad \omega = 0,\quad \Gamma = 0,\quad \frac{\partial \theta}{\partial r}=0 \tag{9}$$

$r = R_C/H, 0 < z < 1$:

$$\psi = 0,\quad \frac{\partial \psi}{\partial r}=\frac{\partial \psi}{\partial z}=0,\quad \Gamma = 0,\quad \theta = 1. \tag{10}$$

Here, A_S and f_S represent the ACRT amplitude and frequency of the rotation rates of the crystal rod, respectively. Another non-dimensional parameter appears in equation (8), which is the Marangoni number $Ma = -(\partial\sigma/\partial T)\Delta TH/\mu\alpha$.

The above equations were solved by adopting a numerical scheme based on a finite-difference scheme. All the computations were conducted on the (41×81) uniform grid network. The Crank–Nicolson scheme was adopted for the unsteady terms. For the convective terms, the HLPA (Hybrid Linear Parabolic Approximation) scheme was utilized [16]. The initial conditions were the solutions for purely natural convection, i.e. the case where the crucible and crystal were stationary. Details of the present numerical procedure were available in Sung *et al.* [14]. The SIP (strongly implicit procedure) solver was employed in numerical computation [17]. The computations were implemented on an HP-715 workstation, and the typical computer CPU time was approximately 8 h for one set of calculations. Convergence was declared when the maximum changes in dimensionless values between two successive iterations were less than 10^{-4}. Several trial calculations were repeated to monitor the sensitivity of the results to the grid size, and the outcome of these tests was satisfactory.

3. RESULTS AND DISCUSSION

The reliability and accuracy of the present simulation were ascertained in the preceding study of Sung *et al.* [14]. In their treatise, the predicted computational results were found to be in agreement with the experimental data of Ozoe *et al.* [15]. As seen in Sung *et al.* [14], the transient temperature oscillation in the melt can be characterized by the dimensionless mixed convection parameter $Ra/(Pr\ Re^2)$. This parameter indicates the relative importance of natural and forced convection. When the buoyancy effect is dominant $[Ra/(Pr\ Re^2) = 0.929]$, temperature rises gradually and afterwards it drops rapidly. If the effect of the forced convection due to the rotation is comparable to the effect of the buoyancy force $[Ra/(Pr\ Re^2) = 0.539]$, the temperature oscillations are in a more organized pattern. For $Ra/(Pr\ Re^2) = 0.225$, in which the forced convection dominates the buoyancy effect, the temperature oscillations are slightly irregular. This is due to the higher rotational speed of the top crystal rod [15]. Based on the flow mode characters pertaining to $Ra/(Pr\ Re^2)$, the main consideration of the present study is to suppress the temperature oscillation by ACRT. The working fluid employed in the present simulation is the same as in Sung *et al.* [14]; the fluid properties are listed in Table 1. The simulation conditions are: $Ra = 1\,694\,600$, $Pr = 4580$, $Ma = 0$ and $0.225 \leqslant Ra/(Pr\ Re^2) \leqslant 0.929$.

Now, the predicted results by the application of ACRT are inspected in Fig. 2 for the case of $Ra/(Pr\ Re^2) = 0.929$, where the buoyancy effect is dominant. As addressed in Sung *et al.* [14], as time progresses, a

Table 1. Properties of the fluid

Properties	Silicon oil
Density (ρ)	971 [kg m^{-3}]
Kinematic viscosity (ν)	5×10^{-4} [m^2]
Volumetric coefficient (β)	9.5×10^{-3} [K^{-1}]
Thermal diffusivity (α)	1.1×10^{-7} [m^2 s^{-1}]

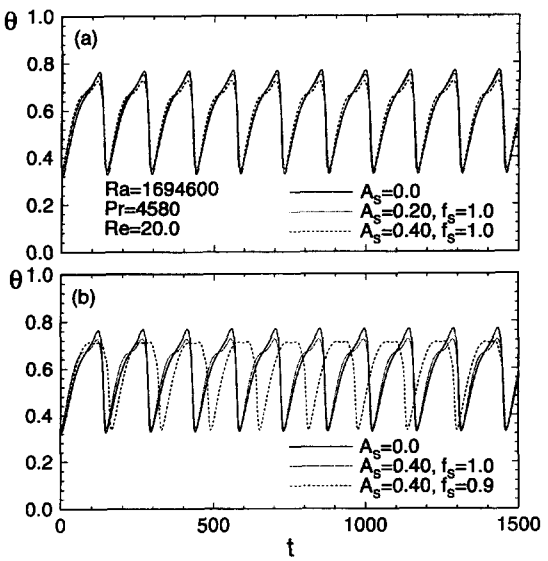

Fig. 2. The effect of (a) A_S on temperature oscillation at $(r,z)=(0,0.7)$ for $Ra/(Pr\ Re^2)=0.929$; (b) f_S on temperature oscillation at $(r,z)=(0,0.7)$ for $Ra/(Pr\ Re^2)=0.929$.

cold plume from the edge of the rotating rod descends periodically to the bottom center of the rotating rod. The buoyancy flow ascending along the crucible wall dominates the cold plume. Near the wall cold flow is concentrated along the periphery of the rotating rod due to the Ekman layer, and the cold plume descends to the bottom center. Consequently, the periodic oscillatory motion sustains a regular pattern. The temperature oscillations at $(r,z)=(0.0,0.7)$ are shown in Fig. 2 for $A_S=0.0$. When ACRT is imposed ($0.0\leqslant A_S\leqslant 0.40$), it is seen that the effect of A_S on θ is not substantial at $f_S=1.0$. Recall that, in applying ACRT, the rotation rate is a function of time, i.e. $\Omega_S=\Omega_{S0}(1+A_S\sin(2\pi/t_p f_S t))$, where Ω_{S0} is the rotation rate of crystal rod without ACRT. If the frequency is changed ($f_S=0.9$), a slight suppression of temperature oscillation is detected. However, the overall impact of ACRT on the suppression of temperature oscillation at $Ra/(Pr\ Re^2)=0.929$ is generally weak.

Next, the present ACRT is employed to the case of $Ra/(Pr\ Re^2)=0.539$, where the buoyancy effect is comparable to the rotation effect. As shown in Fig. 3, the effect of A_S on the temperature oscillation is stronger than for the case of $Ra/(Pr\ Re^2)=0.929$. To quantify the suppression rate of temperature oscillation, a new parameter is defined as $1-\Delta\theta/\Delta\theta_0$. Here, $\Delta\theta_0$ stands for the interval of temperature oscillation when ACRT is not applied, i.e. $\Delta\theta_0=\theta_{max}-\theta_{min}$. In a similar manner, $\Delta\theta$ represents the temperature interval when ACRT is imposed. The suppression rate of temperature oscillation is plotted against A_S in the inset of Fig. 3(a). As is discernible, the maximum suppression takes place at $A_S\cong 0.3$, where the suppression rate is about 20% at $f_S=1.0$, i.e. $1-\Delta\theta/\Delta\theta_0\cong 0.2$. With keeping this optimal value ($A_S=0.3$), the effect of f_S on $1-\Delta\theta/\Delta\theta_0$ is represented in Fig. 3(b). The influence of f_S is also substantial in a broad band of f_S ($0.9\leqslant f_S\leqslant 1.3$). The maximum suppression occurs at $f_S\cong 1.2$, giving the value of $1-\Delta\theta/\Delta\theta_0\cong 0.33$. The time history of temperature oscillation in Fig. 3(b) indicates that, as f_S increases, the period of temperature oscillation decreases slightly.

As shown in the preceding results, the effectiveness of ACRT on the suppression of temperature oscillation is apparent. To scrutinize the detailed flow structures inside the melt, the isolines of meridional temperature (θ) are illustrated in Fig. 4. The time-dependent temperature oscillation (θ) and the corresponding rate (Ω_S) are also displayed in Fig. 5. For comparison, three cases are selected: (a) $A_S=0.0$; (b) $A_S=0.30$, $f_S=1.0$; (c) $A_S=0.30$, $f_S=1.2$. For $A_S=0.0$, as time elapses, the cold plume from the edge of the rotating rod descends periodically to the bottom center of the rotating rod. It is known that the temperature increase in the melt $(r,z)=(0.0,0.7)$ is mainly caused by the rotation due to the Ekman suction, whereas the temperature decrease is governed by the buoyancy force. As shown in Fig. 5(a), the temperature increasing period ($\Delta t\cong 160$, $-50\leqslant t\leqslant 110$) is longer than the temperature decreasing period ($\Delta t\cong 80$, $110\leqslant t\leqslant 190$). This is because the buoyancy flow ascending along the crucible wall dominates the cold plume. The period of temperature oscillation is $t_p\cong 240$. A closer inspection of the isotherm (θ) in Fig. 4(b) for $A_S=0.30, f_S=1.0$ yields that the cold plume is pushed toward the periphery of the crystal rod due to the increased rotation speed of the crystal rod in the early stage of ACRT ($0\leqslant t\leqslant 60$). However, as time elapses ($60\leqslant t\leqslant 180$), the rotation speed is decreased by ACRT. It means that the relative importance of the buoyancy force increases due to the reduced rotation speed. This brings forth the falling of the maximum temperature as compared with the case of $A_S=0.0$. However, as is evident in Fig. 5(b), it is seen that the minimum temperature is maintained as a lower bound. This temperature stagnation is related to the fact that the flow is governed by the augmented buoyancy force. The influence of ACRT on the suppression of temperature oscillation can be seen in Fig. 5(c) for $A_S=0.30, f_S=1.2$. In the early stage of $0\leqslant t\leqslant 100$, the overall rotation speed is decreased due to ACRT. The Ekman suction beneath the crystal rod is attenuated. This gives the rise to a drop of the maximum temperature. In the final stage of $100\leqslant t\leqslant 200$, the rotation speed is increased again by ACRT. However,

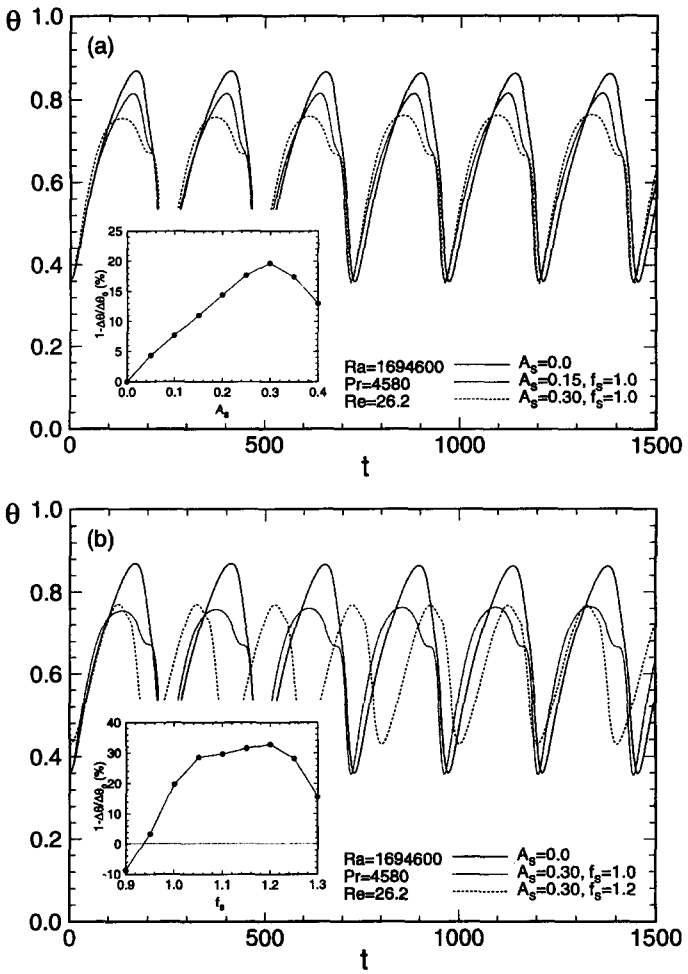

Fig. 3. The effect of (a) A_S on temperature oscillation at $(r, z) = (0, 0.7)$ for $Ra/(Pr\ Re^2) = 0.539$: optimal value of A_S for suppressing temperature oscillation; (b) f_S on temperature oscillation at $(r, z) = (0, 0.7)$ for $Ra/(Pr\ Re^2) = 0.539$: optimal value of f_S for suppressing temperature oscillation.

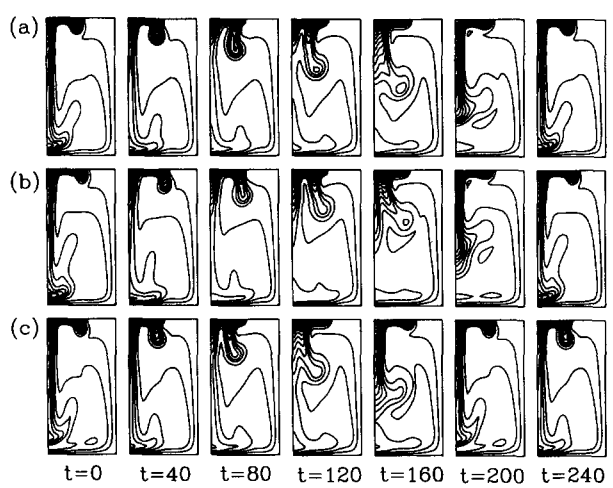

Fig. 4. Contour plots of isotherms (θ) in the meridional plane for $Ra/(Pr\ Re^2) = 0.539$ (a) $A_S = 0.0$; (b) $A_S = 0.3, f_S = 1.0$; (c) $A_S = 0.3, f_S = 1.2$.

the increase of temperature does not catch up with the increase of rotation speed in time. As shown in Fig. 5(c), a time lag ($t_p/4$) is clearly displayed and the total period of temperature oscillation is about $t_p \cong 200$. Due to an excessive evolution of ACRT in time, the lower bound temperature is also pulled up. This leads

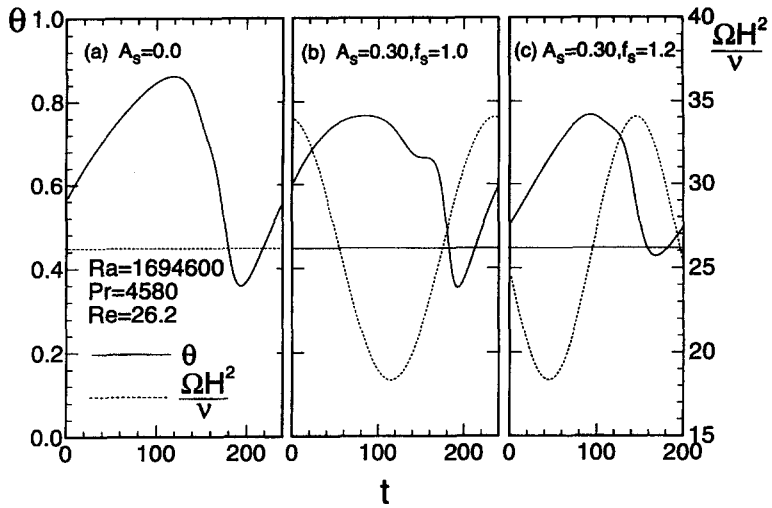

Fig. 5. The relation between the rotation rate of crystal rod (Ω_S) and temperature oscillation (θ) for $Ra/(Pr\ Re^2) = 0.539$: (a) $A_S = 0.0$; (b) $A_S = 0.3, f_S = 1.0$; (c) $A_S = 0.3, f_S = 1.2$.

to the maximum suppression of temperature oscillation.

The results pertaining to the case of $Ra/(Pr\ Re^2) = 0.225$ are exhibited in Fig. 6, where the forced convection dominates the buoyancy effect. The influence of ACRT on the suppression of temperature oscillation is seen to be remarkable. In particular, the suppression rate of temperature oscillation as $A_S = 0.15, f_S = 1.0$ reaches 90%, i.e. $1 - \Delta\theta/\Delta\theta_0 \cong 0.9$. As compared with the previous cases, it is evident that the application of ACRT is more effective in the forced-convection dominant regime than in the buoyancy-effect dominant regime. This is caused by the fact that the present ACRT, by imposing the variation of rotation rate of crystal rod, can give a direct impact on the forced convection dominant regime rather than on the natural convection dominant regime.

To characterize the salient influence of ACRT in the forced-convection dominant regime, the isolines of meridional temperature was illustrated in Fig. 7. When ACRT is not applied ($A_S = 0.0$), it is seen that a cold plume starts to descend from the periphery of the rotating rod in a balloon-shape. As time elapses, the balloon-shaped fluid becomes colder due to the cold bottom plane of the top cylinder. The hot fluid under this balloon-shaped fluid breaks upwards and flows in the central region below the crystal rod. Since the hot fluid is entrained from the wall, the time-averaged melt temperature at $(r, z) = (0.0, 0.7)$ is raised as compared with the preceding one (Fig. 3). Moreover, the cold plume rapidly disappears. This gives rise to a narrow temperature interval ($\Delta\theta_0$), as shown in Fig. 6. Next, when ACRT is imposed as $A_S = 0.15$, $f_S = 1.0$, the overall transient modes of temperature are similar to the previous one ($A_S = 0.0$). However, due to a higher rotation speed ($Re = 40.6$), the cold plume descends far away from the center and then it returns slowly to the center. A closer inspection of the transient flow mode in Fig.

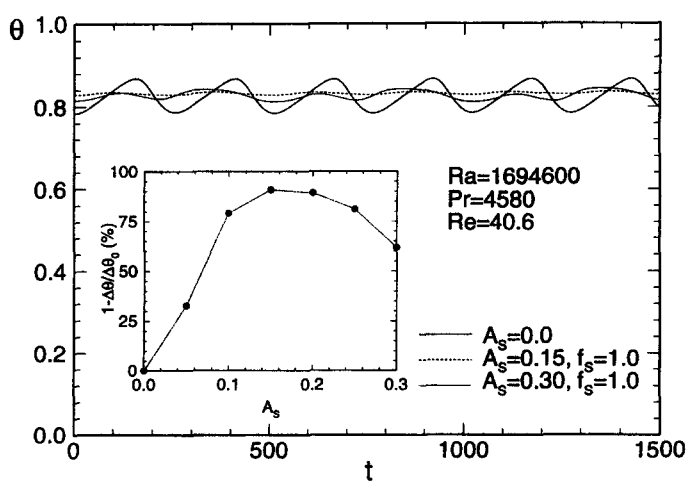

Fig. 6. The effect of A_S on temperature oscillation at $(r, z) = (0, 0.7)$ for $Ra/(Pr\ Re^2) = 0.225$: optimal value of A_S for suppressing temperature oscillation.

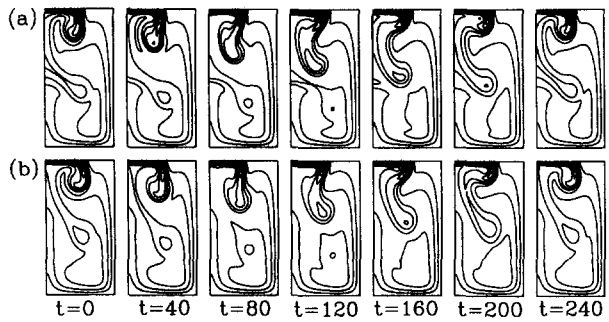

Fig. 7. Contour plots of isotherms (θ) in the meridional plane for $Ra/(Pr\ Re^2) = 0.225$: (a) $A_S = 0.0$; (b) $A_S = 0.15, f_S = 1.0$.

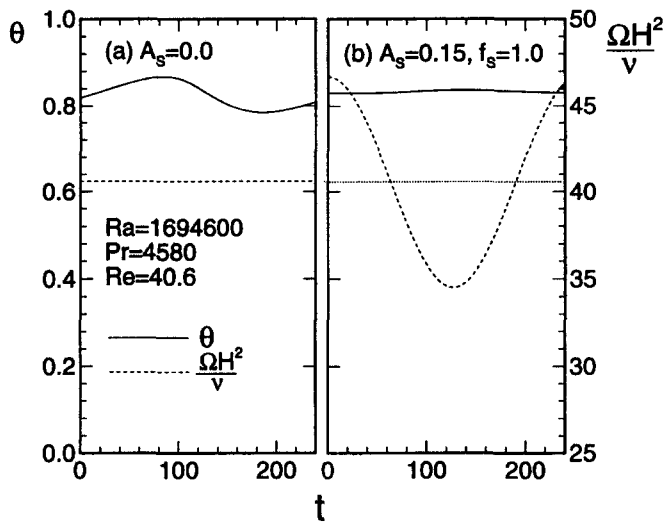

Fig. 8. The relation between the rotation rate of crystal rod (Ω_S) and temperature oscillation (θ) for $Ra/(Pr\ Re^2) = 0.225$: (a) $A_S = 0.0$; (b) $A_S = 0.15, f_S = 1.0$.

7(b) discloses that the cold plume never collides with the center line, i.e. the position $(r, z) = (0.0, 0.7)$. As shown in Fig. 8(a), the temperature is increased at the early stage of ACRT ($0 \leqslant t \leqslant 80$). However, for the case of $A_S = 0.15, f_S = 1.0$, this stage is equivalent to the step when the rotation is increased. This means that the cold plume descends vertically without the influence of temperature oscillation. In the final stage of ACRT ($80 \leqslant t \leqslant 160$), although the buoyancy effect is slightly strengthened due to the decrease of rotation speeds, the cold plume does not give influence on the temperature oscillation at the position $(r, z) = (0.0, 0.7)$.

A major complication in the analysis of convection and striation in melt crystal growth is the need for simultaneous calculation of the melt/crystal interface shape with temperature, velocity and pressure fields [18]. Since the assumption of local thermal equilibrium is adopted in the present simulation due to lower growth rates, the menuiscus is represented by an orthogonal coordinate system, i.e. plane. However, macroscopic details of the melt/crystal interface structure depend crucially on the surface temperature distribution in the radial direction [19]. To look into the spatial uniformity of temperature, the distributions of temperature are exhibited in Fig. 9, where the temperature is visualized in time (t) and space (r) at the near interface surface ($z = 0.95$). For $A_S = 0.0$, the distribution of temperature in the region ($0 \leqslant r \leqslant 0.15$) is seen to be nearly uniform in space, as shown in Fig. 9(a). But, the temperature is oscillated in time. Outside the crystal rod ($0.15 \leqslant r \leqslant 0.25$) the temperature drops significantly. When ACRT is imposed ($A_S = 0.15, f_S = 1.0$), as is discernible in Fig.

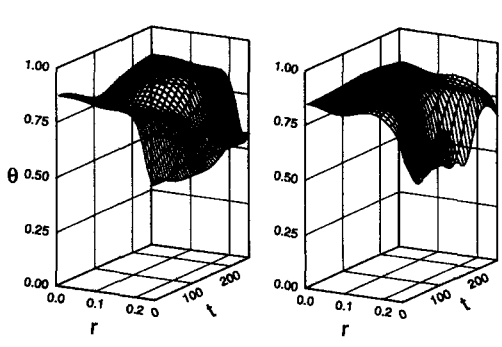

Fig. 9. The temperature distribution in space and in time near the crystal/melt interface for $Ra/(Pr\ Re^2) = 0.225$: (a) $A_S = 0.0$; (b) $A_S = 0.15, f_S = 1.0$.

Table 2. Effect of crystal radius on $1-\Delta\theta/\Delta\theta_0$

	Re		
R_S/R_C	20.0	26.2	40.6
4/8	14.9%	32.8%	90.8%
5/8	25.0%	37.8%	39.3%

9(b), the temperature is uniform in space and in time. This is mainly attributed to the Ekman layer due to the rotation. However, the uniformity is confined to the region beneath the crystal rod. Outside the crystal rod ($0.15 \leqslant r \leqslant 0.25$), a significant temperature variation is seen. This big change in temperature is caused by the tip vorticity, which is generated at the end periphery of the crystal rod. The Ekman layer is broken due to the periodic motion of balloon-shaped cold plume in the periphery of crystal rod. The lower heat transfer rate prevents the balloon-shaped cold plume from being reheated relatively.

Much effort has been given to producing large-sized crystals to increase the productivity of semiconductors in industry. Thus, the crystal radius is enlarged from 4/8 to 5/8, where the value indicates the ratio of the crystal radius (R_S) to the crucible radius (R_C). The effects of crystal radius on $1-\Delta\theta/\Delta\theta_0$ are summarized in Table 2, where three Reynolds numbers are employed for comparison. As the Reynolds number increases, the influence of ACRT on the suppression of temperature oscillation also increases. As the crystal radius is enlarged, the result is not consistent. However, the overall trend is similar, i.e. the suppression rate by ACRT is more effective in the forced-convection dominant regime than in the natural-convection dominant regime.

As stressed earlier, from the standpoint of industrial application of ACRT, the attainment of $(1-\Delta\theta/\Delta\theta_0)_{max}$ is a primary goal. However, all the prior values of $1-\Delta\theta/\Delta\theta_0$ have been obtained at the position $(r,z)=(0.0,0.7)$. The main reason to select this position was to extend a comparison with the experimental data [15]. The temperature oscillations at different positions for $Ra/(Pr\,Re^2)=0.539$ are illustrated in Fig. 10, where the measuring points are: $(r,z)=(0.0,0.9)$ and $(r,z)=(0.3,0.9)$. The position $(r,z)=(0.0,0.9)$ represents the position close to the interface beneath the crystal rod, while the position $(r,z)=(0.3,0.9)$ is located beyond the crystal rod region. It is evident in Fig. 10 that the suppression by ACRT is more effective in the position $(r,z)=(0.0,0.9)$ than in the position $(r,z)=(0.3,0.9)$. Furthermore, it is seen that, at the position $(r,z)=(0.3,0.7)$, the suppression of temperature oscillation by ACRT is deteriorated than that without ACRT.

4. CONCLUSION

Based on the inherent transient oscillatory flow modes in Czochralski convection, the present ACRT has been applied to suppress the temperature oscillation in the melt. By altering the rotation rate of the crystal rod, a suppression of temperature oscillation has been accomplished. The suppression rate of temperature oscillation by ACRT can be characterized by the dimensionless mixed convection parameter $[Ra/(Pr\,Re^2)]$. When the buoyancy effect is dominant, the impact of ACRT is generally weak. The application of ACRT is more effective in the forced-convection dominant regime than in the buoyancy-convection dominant regime. In particular, for $Ra/(Pr\,Re^2)=0.225$, where the forced-convection dominates the buoyancy effect, the suppression rate of temperature oscillation at $A_S=0.15$, $f_S=1.0$ reaches 90%, i.e. $1-\Delta\theta/\Delta\theta_0 \cong 0.9$. When ACRT is imposed, the temperature distribution near the interface becomes uniform in the radial direction. However, the uniformity by ACRT is restricted within the region beneath the crystal rod ($0 \leqslant r \leqslant 0.15$).

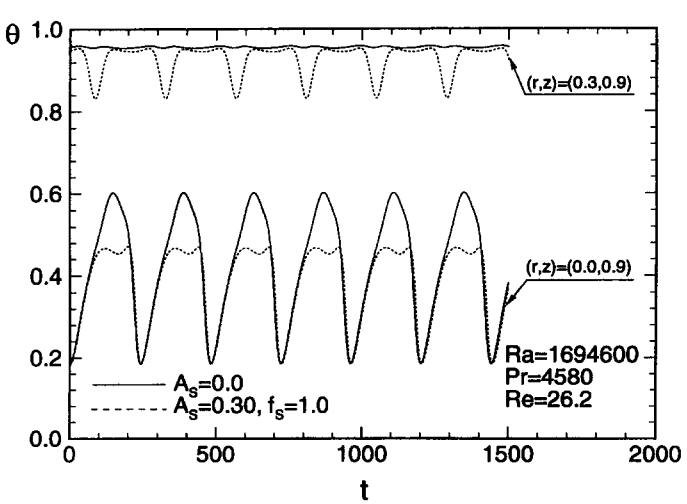

Fig. 10. The effect of ACRT on temperature oscilltion at $(r,z)=(0.3,0.9)$ and $(r,z)=(0.0,0.9)$ for $Ra/(Pr\,Re^2)=0.539$: (a) $A_S=0.0$; (b) $A_S=0.30, f_S=1.0$.

REFERENCES

1. Langlois, W. E., Conservative differencing procedures for rotationally symmetric flow with swirl. *Computational Method in Applied Mechanical Engineering*, 1981, **25,** 315–333.
2. Kishino, S., Kamamori, M., Yoshihiro, N., Tajima, M., and Lizuka, T., Heat treatment behavior of microdefects and residual impurities in Cz silicon crystals. *Journal of Applied Physics*, 1979, **50,** 8240–8243.
3. Utech, H. P., and Flemings, M. C., Elimination of solute banding in indium antimonide crystals by growth in a magnetic field. *Journal of Applied Physics*, 1966, **37,** 2021–2024.
4. Langlois, W. E., Buoyancy-driven flows in crystal-growth melts. *Annual Review of Fluid Mechanics*, 1985, **17,** 191–215.
5. Series, R. W., and Hurle, D. T. J., The use of magnetic fields in semiconductor crystal growth. *Journal of Crystal Growth*, 1991, **113,** 305–328.
6. Chedzey, H. A., and Hurle, D. T. J., Avoidance of growth-striate in semiconductor and metal crystals grown by zone-melting techniques. *Nature*, 1966, **210,** 933–934.
7. Munakata, T., and Tanasawa, I., Onset of oscillatory flow in a Czochralski growth melt and its suppression by magnetic field. *Journal of Crystal Growth*, 1990, **106,** 566–576.
8. Scheel, H. J., and Mueller-Krumbhaar, H., Crystal pulling using ACRT, *Journal of Crystal Growth*, 1980, **49,** 291–296.
9. Mihelčić, M., Schröck-pauli, C., Wingerth K., Wenzl, H., Uelhoff, W., and Van der Hart, A., Numerical simulation of forced convection in the classical Czochralski method in ACRT and CACRT, *Journal of Crystal Growth*, 1981, **53,** 337–354.
10. Mihelčić, M., Schröck-pauli, C., Wingerth, K., Wenzl, H., Uelhoff, W., and Van der Hart, A., Numerical simulation of free and forced convection in the classical Czochralski method and in CACRT. *Journal of Crystal Growth*, 1982, **57,** 300–317.
11. Rappl, P. H. O., Matteo, L. F., Scheel, H. J., Barros, M. R. X., and Schiel, D., Hydrodynamic simulation of forced convection in Czochralski and melts. *Journal of Crystal Growth*, 1984, **70,** 49–55.
12. Scheel, H. J., and Schulz-Dubois, E. O., Flux growth of large crystals by accelerated crucible rotation technique. *Journal of Crystal Growth*, 1971, **8,** 304–306.
13. Scheel, H. J., Accelerated crucible rotation : a novel stirring technique in high temperature solution growth. *Journal of Crystal Growth*, 1972, **13/14,** 560–565.
14. Sung, H. J., Jung, Y. J., and Ozoe, H., Prediction of transient oscillatory flow in Czochralski convection. *International Journal of Heat and Mass Transfer*, 1995, **38,** 1627–1636.
15. Ozoe, H., Toh, K., and Inoue, T., Transition mechanism of modes in Czochralski convection. *Journal of Crystal Growth*, 1991, **110,** 472–480.
16. Zhu, J., On the higher-order bounded discretization schemes for finite volume computations of incompressible flows. *Computational Method in Applied Mechanical Engineering*, 1992, **98,** 345–360.
17. Stone, H. L., Iterative solution of implicit approximations of multidimensional partial differential equations. *SIAM Journal of Numerical Analysis*, 1968, **5,** 530–558.
18. Brown, R. A., Theory of transport process in single crystal growth from the melt. *A.I.Ch.E. Journal*, 1988, **34,** 881–911.
19. Kobayashi, N., Computational simulation of the melt flow during Czochralski growth. *Journal of Crystal Growth*, 1978, **43,** 357–363.